



Numerical treatment of activation energy for the three-dimensional flow of a cross magnetonanoliquid with variable conductivity

S MUHAMMAD¹, G ALI¹, S I A SHAH¹, M IRFAN², W A KHAN^{3,*}, M ALI³ and F SULTAN³

¹Department of Mathematics, Islamia College, Peshawar 25000, Pakistan

²Department of Mathematics, Quaid-i-Azam University, Islamabad 44000, Pakistan

³Department of Mathematics, Hazara University, Mansehra 21300, Pakistan

*Corresponding author. E-mail: waqar_qau85@yahoo.com

MS received 17 May 2018; revised 3 January 2019; accepted 20 February 2019; published online 17 June 2019

Abstract. This research demonstrates the diverse characteristics of the cross fluid in the presence of Lorentz's forces. Moreover, this work reviews the characteristics of variable diffusivity and variable conductivity. Mathematical modelling of the presented physical model is carried out in the Cartesian coordinate system and the formulated system of partial differential equations (PDEs) is simplified in ordinary differential equations (ODEs). Numerical algorithm leads to solution computations. Velocity, temperature and concentration are numerically analysed for the cross fluid. Outcomes of the current physical model are presented through graphical data and in tabular form. It is noted that variable conductivity and variable diffusivity significantly affect heat–mass transport mechanisms. Furthermore, graphical analysis reveals that the concentration of the cross nanofluid increase for increased values of variable diffusivity. Furthermore, this research reveals that concentration distribution is a reducing function of chemical reaction parameters.

Keywords. Three-dimensional flow; variable conductivity; variable diffusivity; activation energy.

PACS Nos 02.30.Hq; 02.30.Jr; 05.40.Jc; 44.10.+i; 47.10.A–

1. Introduction

Lubricants and coolant liquids are utilised in various industrial applications. The efficiency and development of heat transport devices mainly depend on thermal conductivity of these liquids. This is the most significant goal for these technologies to be financially and energetically viable. Furthermore, in the available literature, there are various procedures that enhance the heat transport coefficient of the flow and improve the efficiency of the solar collector. Solid nanoparticles have higher thermal conductivity when compared to base liquids. Therefore, the idea of adding solid nanoparticles into base liquid was considered. Nanoliquids are utilised inside an absorber and serve as heat transfer liquids. Nanoliquids possess superior thermal features and enhance the performance of the solar system. Khan *et al* [1] considered the impact of nanoparticles on an Oldroyd-B fluid in the presence of a heat sink–source. Gupta and Ray [2] inspected the features of squeezing the time-dependent flow between parallel plates in the presence of nanoparticles. Sheikholeslami and Ellahi [3] studied

the characteristics of cubic cavity for three-dimensional (3D) flow of the magnetonanoliquid. Khan and Khan [4] performed the analysis of Burgers' fluid in the presence of nanoparticles. Sandeep *et al* [5] investigated the impact of convective heat/mass transfer mechanisms on non-Newtonian magnetonanoliquid. Khan and Khan [6] deliberated the impact of the no-mass flux condition on the power law of nanofluids. Haq and Khan [7] considered a two-phase model with water and ethylene glycol-based Cu nanoparticles under suction–injection. A steady-state two-dimensional (2D) flow of Burgers' fluid in the presence of nanoparticles was demonstrated by Khan and Khan [8]. Zero mass flux relation has been employed by Khan *et al* [9] to visualise the behaviour of Burgers' fluid in the presence of nanoparticles. Rahman *et al* [10] reported nanofluid flow for Jeffrey fluid. Raju *et al* [11] studied the magnetonanoliquid flow in the presence of a rotating cone with temperature-dependent viscosity. Recently, several researchers published their work on heat transport [11–31].

Chemical reactions can be categorised into different types such as homogeneous/heterogeneous reactions,

catalytic/non-catalytic reactions, single-step/multistep reactions, etc. Mostly, the reactions are complex in nature; they proceed through a reaction mechanism or just a mechanism consisting of a number of chemical reaction steps, or the so-called elementary steps. To reduce the complexity of complex reactions, mathematical modelling is essential. Mathematical chemistry deals with the mathematical modelling of chemical phenomena while computational chemistry applies computer techniques to assist in solving chemical problems. It is necessary in today’s science to study chemical processes and reaction rates, to analyse the structures and properties of atoms and molecules, to simulate, optimise and control the processes. In fact, it allows us to study different factors affecting the speed of chemical reactions and gives information about the whole mechanism and transition states. Today we can talk about the microscopic or molecular level of each reaction, i.e. activation energy, atomic collision, at different stages during the reaction. An analysis of the detailed reaction mechanism of the complete interaction between the heat transfer behaviour and cracking reactions offers deep insights. Khan *et al* [32] analysed the chemical phenomenon for the 3D flow of a non-Newtonian nanofluid. Khan *et al* [33] investigated the characteristics of chemical processes on 3D flow of Burgers’ fluid. Khan *et al* [34] explored the features of convective flow in the presence of a surface with variable thickness. Khan *et al* [35] inspected the aspects of chemical mechanisms by utilising a revised relation. Khan *et al* [36] scrutinised the impact of chemical reactions on generalised Burgers’ nanofluid. Mustafa *et al* [37] examined the characteristics of activation energy and chemical mechanisms on the magnetonanofluid. Khan *et al* [38] studied the aspects of autocatalysis chemical reaction in nonlinear radiative 3D flow of the cross magnetofluid.

Based on the aforementioned literature reviews, we perceived that scant consideration has been paid to the 3D flow of a cross nanofluid over a bidirectional stretched surface. Mathematical modelling of the presented physical model is conducted by considering the aspects of no-flux condition at the boundary. Moreover, heat–mass transport mechanisms are carried out by utilising characteristics of activation energy and Lorentz’s forces. MATLAB function bvp4c scheme is implemented to obtain numerical solutions of the presented physical model. The impacts of the involved physical parameters on the flow and heat–mass transport characteristics are presented using tables and graphs.

2. Modelling

Three-dimensional flow of an incompressible cross fluid in the presence of nanoparticles is reviewed. The configuration of the present physical model is presented in figure 1. Moreover, the flow through the medium is caused by a stretched surface and restricted in the domain, $z > 0$. Heat sink–source mechanisms are carried out in current physical situation which has some engineering applications, such as dissociating fluid. Heat–mass transport mechanisms are examined using variable diffusivity and variable conductivity. A non-uniform magnetic field is applied in the z direction. Moreover, simulation is performed by assuming low Reynolds number. Convective heat transport and no-mass flux conditions are encountered. The governing equations under the above stated assumptions are as follows:

$$\frac{\partial u}{\partial x} + \frac{\partial v}{\partial y} + \frac{\partial w}{\partial z} = 0, \tag{1}$$

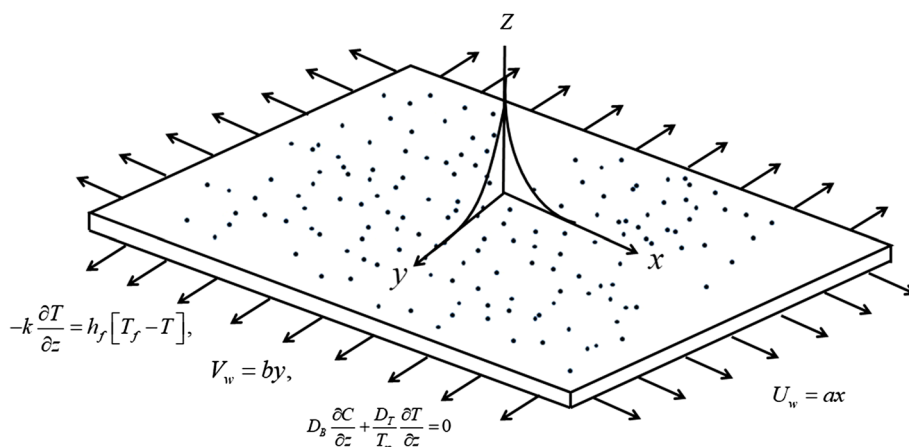


Figure 1. Flow geometry.

$$\begin{aligned}
 u \frac{\partial u}{\partial x} + v \frac{\partial u}{\partial y} + w \frac{\partial u}{\partial z} &= -\frac{1}{\rho_f} \frac{\partial P}{\partial x} + v \frac{\partial}{\partial z} \left[\frac{(\partial u / \partial z)}{1 + \{\Gamma(\partial u / \partial z)\}^n} \right] - \frac{\sigma^* B_0^2 u}{\rho_f}, \\
 &+ \tau \left[D_B \frac{\partial C}{\partial z} \frac{\partial T}{\partial z} + \frac{D_T}{T_\infty} \left(\frac{\partial T}{\partial z} \right)^2 \right] \\
 &+ \frac{Q_0}{(\rho c)_f} (T - T_\infty). \tag{10}
 \end{aligned}$$

$$\begin{aligned}
 u \frac{\partial v}{\partial x} + v \frac{\partial v}{\partial y} + w \frac{\partial v}{\partial z} &= -\frac{1}{\rho_f} \frac{\partial P}{\partial y} + v \frac{\partial}{\partial z} \left[\frac{(\partial v / \partial z)}{1 + \{\Gamma(\partial v / \partial z)\}^n} \right] - \frac{\sigma^* B_0^2 v}{\rho_f}, \tag{2} \\
 & \tag{3}
 \end{aligned}$$

$$\begin{aligned}
 u \frac{\partial T}{\partial x} + v \frac{\partial T}{\partial y} + w \frac{\partial T}{\partial z} &= \frac{1}{(\rho c)_f} \frac{\partial}{\partial z} \left(k(T) \frac{\partial T}{\partial z} \right) \\
 &+ \tau \left[D_B \frac{\partial C}{\partial z} \frac{\partial T}{\partial z} + \frac{D_T}{T_\infty} \left(\frac{\partial T}{\partial z} \right)^2 \right] \\
 &+ \frac{Q_0}{(\rho c)_f} (T - T_\infty), \tag{4}
 \end{aligned}$$

$$\begin{aligned}
 u \frac{\partial C}{\partial x} + v \frac{\partial C}{\partial y} + w \frac{\partial C}{\partial z} &= \frac{\partial}{\partial z} \left(D_B(C) \frac{\partial C}{\partial z} \right) + \frac{D_T}{T_\infty} \frac{\partial^2 T}{\partial z^2} \\
 &- k_c^2 (C - C_\infty) \left(\frac{T}{T_\infty} \right)^m \exp \left(-\frac{E_a}{KT} \right) \tag{5}
 \end{aligned}$$

with

$$u = U_w = ax, \quad v = V_w = by, \quad w = 0,$$

$$-k \frac{\partial T}{\partial z} = h_f [T_f - T],$$

$$D_B \frac{\partial C}{\partial z} + \frac{D_T}{T_\infty} \frac{\partial T}{\partial z} = 0 \quad \text{at } z = 0,$$

$$u \rightarrow 0, \quad v \rightarrow 0, \quad T \rightarrow T_\infty,$$

$$C \rightarrow C_\infty \quad \text{as } z \rightarrow \infty, \tag{7}$$

where

$$k(T) = k_\infty \left(1 + \varepsilon_1 \left(\frac{T - T_\infty}{T_f - T_\infty} \right) \right), \tag{8}$$

$$D(C) = k_\infty \left(1 + \varepsilon_2 \left(\frac{C - C_\infty}{C_\infty} \right) \right), \tag{9}$$

Utilising eqs (8) in (4) and eqs (9) in (5), we get

$$\begin{aligned}
 u \frac{\partial T}{\partial x} + v \frac{\partial T}{\partial y} + w \frac{\partial T}{\partial z} &= \frac{1}{(\rho c)_f} \frac{\partial}{\partial z} \left(k(T) \frac{\partial T}{\partial z} \right)
 \end{aligned}$$

Consider

$$u = axf'(\eta), \quad v = ayg'(\eta),$$

$$w = -(av)^{1/2} [f(\eta) + g(\eta)],$$

$$\theta(\eta) = \frac{T - T_\infty}{T_f - T_\infty}, \quad \varphi(\eta) = \frac{C - C_\infty}{C_\infty},$$

$$\eta = z \sqrt{\frac{a}{\nu}}. \tag{11}$$

The requirement of continuity equation is automatically fulfilled by utilising transformation (11), whereas eqs (2)–(7), (9) and (10) take the form

$$\begin{aligned}
 [1 + (1 - n)(We_1 f'')^n] f''' - [1 + (We_1 f'')^n]^2 \\
 \times [f'^2 - (f + g)f'' + M^2 f'] = 0, \tag{12}
 \end{aligned}$$

$$\begin{aligned}
 [1 + (1 - n)(We_2 g'')^n] g''' - [1 + (We_2 g'')^n]^2 \\
 \times [g'^2 - (f + g)g'' + M^2 g'] = 0, \tag{13}
 \end{aligned}$$

$$\begin{aligned}
 (1 + \varepsilon_1 \theta) \theta'' + \varepsilon_1 \theta'^2 + Pr[(f + g)\theta' + N_b \theta' \varphi' \\
 + N_t \theta'^2] + Pr \lambda \theta = 0, \tag{14}
 \end{aligned}$$

$$\begin{aligned}
 (1 + \varepsilon_2 \varphi) \varphi'' + \varepsilon_2 \varphi'^2 + Le Pr (f + g) \varphi' \\
 - Le Pr \sigma \varphi (1 + \delta \theta)^m \exp \left(-\frac{E}{1 + \delta \theta} \right) + \frac{N_t}{N_b} \theta'' = 0, \tag{15}
 \end{aligned}$$

$$f = 0, \quad g = 0, \quad f' = 1, \quad g' = \alpha,$$

$$\theta'(0) = -\gamma [1 - \theta(0)],$$

$$N_b \varphi'(0) + N_t \theta'(0) = 0 \quad \text{at } \eta = 0, \tag{16}$$

$$f' \rightarrow 0, \quad g' \rightarrow 0, \quad \theta \rightarrow 0, \quad \varphi \rightarrow 0, \quad \text{as } \eta \rightarrow \infty. \tag{17}$$

Dimensionless physical parameters are defined as

$$We_1 = \Gamma ax \sqrt{\frac{a}{\nu}}, \quad We_2 = \Gamma ay \sqrt{\frac{a}{\nu}}, \quad \alpha = \frac{b}{a},$$

$$M = \frac{\sigma^* B_0^2}{\rho_f a}, \quad N_b = \frac{\tau D_B C_\infty}{\nu},$$

$$N_t = \frac{\tau D_T (T_f - T_\infty)}{\nu T_\infty}, \quad \lambda = \frac{Q_0}{a(\rho c)_f},$$

$$Pr = \frac{\nu}{\alpha_1}, \quad Le = \frac{\alpha_1}{D_B}, \quad \sigma = \frac{k_c^2}{a},$$

$$E = \frac{E_a}{k_\infty T_\infty}, \quad \delta = \frac{T_f - T_\infty}{T_\infty}. \tag{18}$$

3. Quantities of interest

Mathematically, the expression for surface drag forces and heat transport rate are defined as

$$C_{f_x} = \frac{2\tau_{xz}}{\rho_f U_w^2}, \quad C_{f_y} = \frac{2\tau_{yz}}{\rho_f U_w^2}, \quad (19)$$

$$\text{Nu}_x = -\frac{x}{(T_f - T_\infty)} \left(\frac{\partial T}{\partial z} \right) \Big|_{z=0}. \quad (20)$$

In dimensionless form, one has

$$C_{f_x} (\text{Re}_x)^{1/2} = \frac{2f''(0)}{[1 + (\text{We}_1 f''(0))^n]}, \quad (21)$$

$$C_{f_y} (\text{Re}_y)^{-1/2} = \frac{2V_w g''(0)}{U_w [1 + (\text{We}_2 g''(0))^n]}, \quad (22)$$

$$(\text{Re}_x)^{-1/2} \text{Nu}_x = -\theta'(0), \quad (22)$$

where

$$\text{Re}_x = \frac{ax^2}{\nu}.$$

4. Solution of the proposed problem

The nonlinear ODEs along with the associated conditions are integrated by utilising MATLAB tool bvp4c. The ruling ODEs are converted into first-order ODEs and MATLAB software bvp4c is implemented for the step by step integration.

4.1 Verification of numerical outcomes

Table 1 provides a comparison of the current numerical data with the existing literature for the Newtonian fluid tabulated by Ariel [39]. The numerical data for $-f''(0)$

Table 1. Comparison of surface drag forces for the Newtonian liquid ($\text{We}_1 = \text{We}_2 = M = 0$).

α	HPM result [37]	HPM result [37]	Present result	Present result
	$-f''(0)$	$-g''(0)$	$-f''(0)$	$-g''(0)$
0.0	1.0	0.0	1.0	0.0
0.1	1.02025	0.06684	1.02026	0.06685
0.2	1.03949	0.14873	1.03949	0.14874
0.3	1.05795	0.24335	1.05795	0.24336
0.4	1.07578	0.34920	1.07578	0.34921
0.5	1.09309	0.46520	1.09309	0.46521
0.6	1.10994	0.59052	1.10994	0.59053
0.7	1.12639	0.72453	1.12639	0.72453
0.8	1.14248	0.86668	1.14249	0.86668
0.9	1.15825	1.01653	1.15826	1.016538
1.0	1.17372	1.17372	1.17372	1.17372

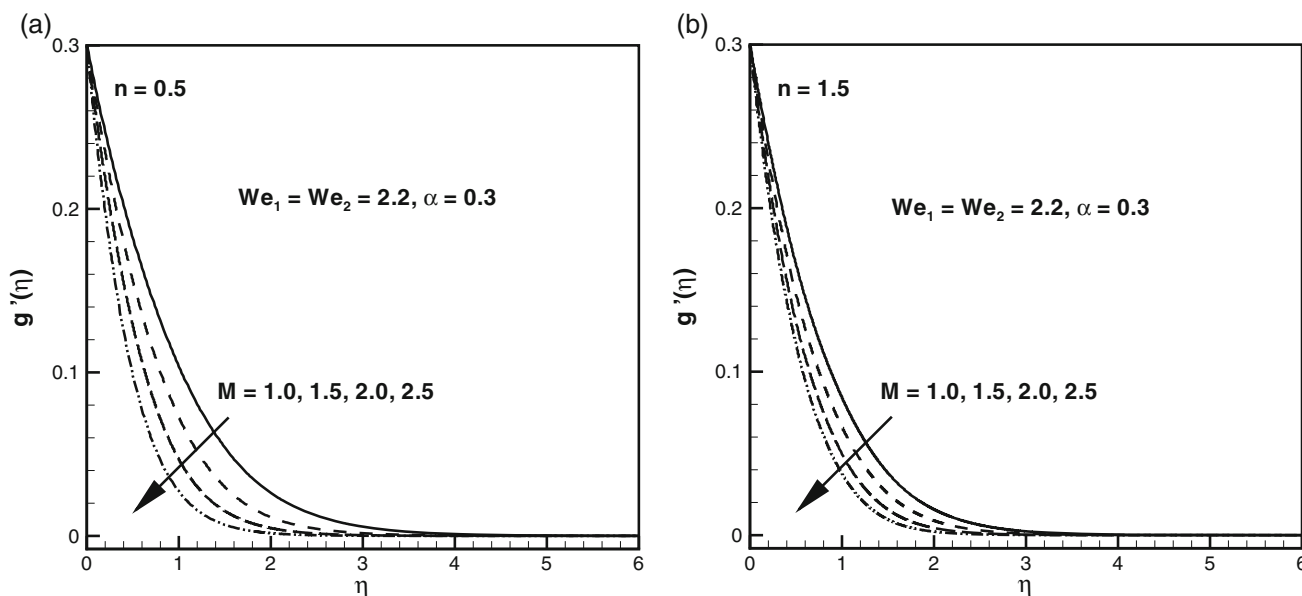


Figure 2. Illustration of $g'(\eta)$ for various values of M for (a) shear-thinning and (b) shear-thickening liquids.

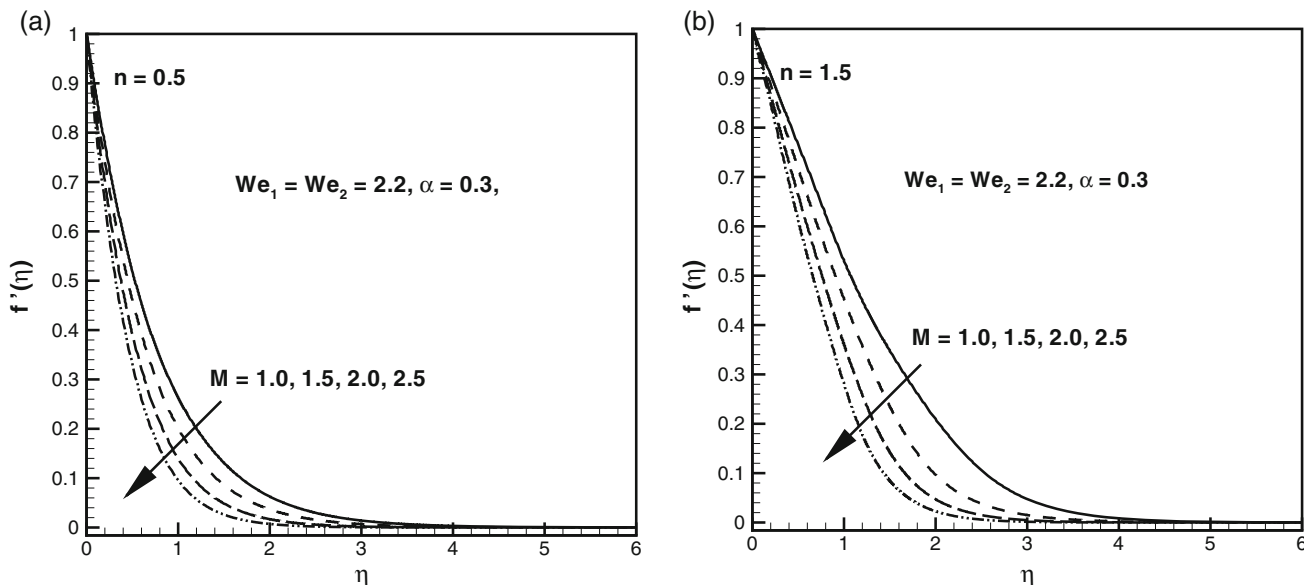


Figure 3. Illustration of $f'(\eta)$ for various values of M for (a) shear-thinning and (b) shear-thickening liquids.

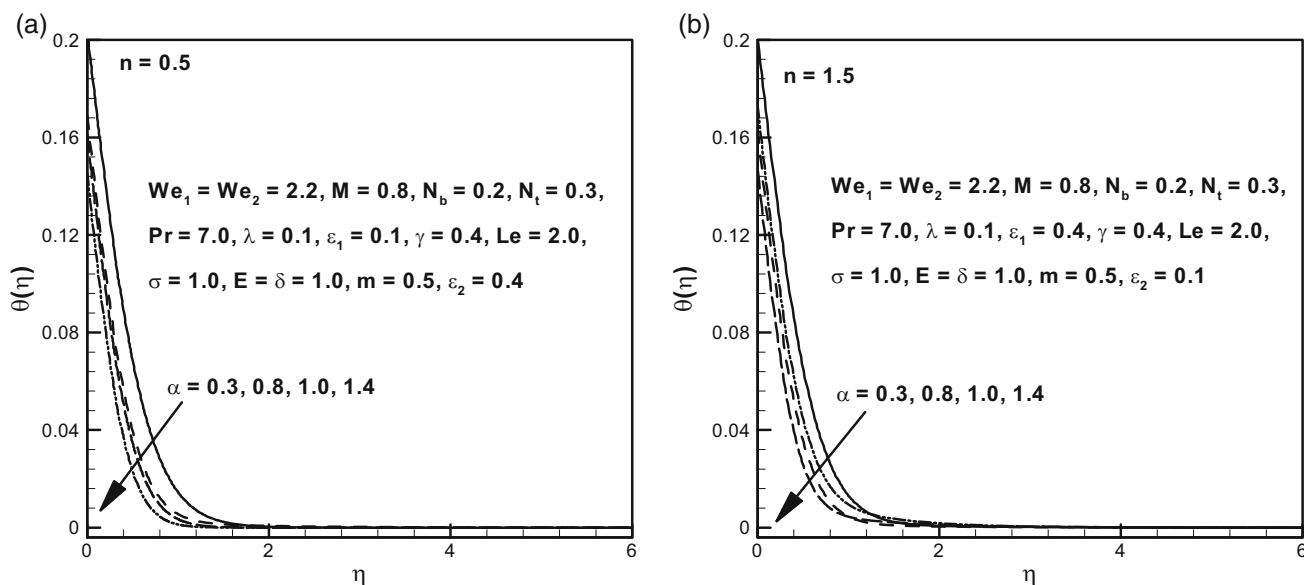


Figure 4. Illustration of $\theta(\eta)$ for various values of α for (a) shear-thinning and (b) shear-thickening liquids.

and $-g''(0)$ are computed and the legitimacy of the work is ensured.

5. Discussion

The main theme here is to mark the physical interpretation of the behaviour of various physical parameters which arise in the flow, heat and mass transport of the cross magnetonanofluid past a bidirectional stretched surface. The numerical technique, namely, *bvp4v* is employed to integrate the governing physical model.

The main motivation behind the current research work is to investigate the aspects of all the involved physical parameters such as velocity, temperature and nanofluid concentration profiles. Moreover, flow and heat transport mechanisms are probed by computing the value of drag forces and Nusselt number.

5.1 Nanofluid velocity profiles

Figures 2a, 2b and 3a, 3b demonstrate the impact of M on the velocity of the cross nanofluid. For a stretched surface, increasing M leads to the deterioration of the

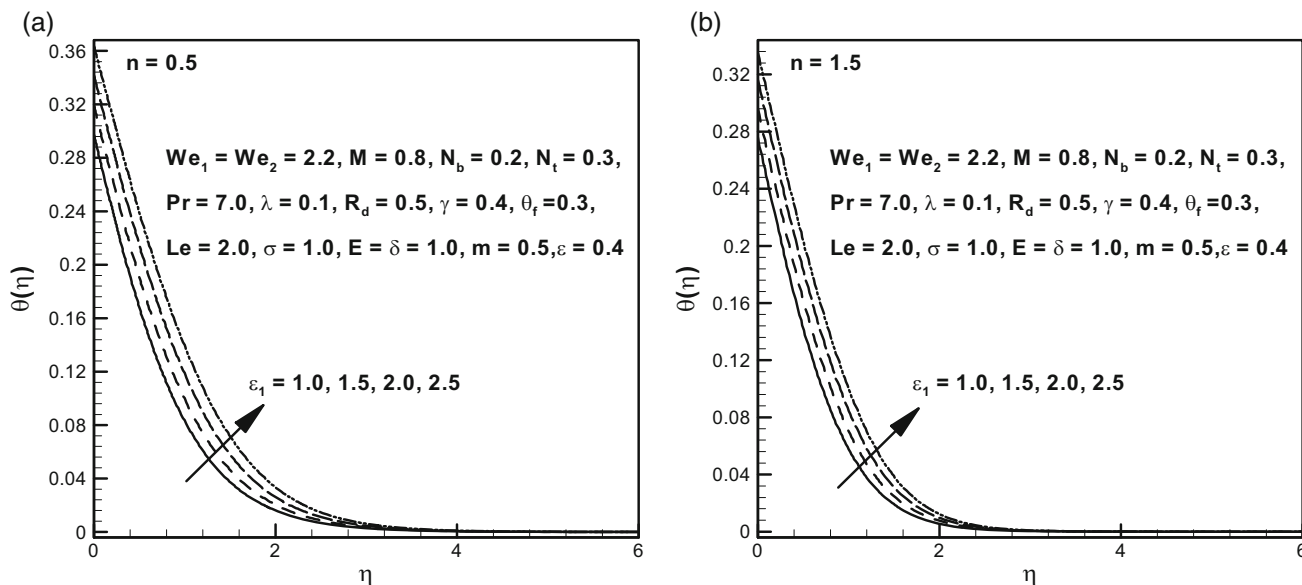


Figure 5. Illustration of $\theta(\eta)$ for various values of ϵ_1 for (a) shear-thinning (b) and shear-thickening liquids.

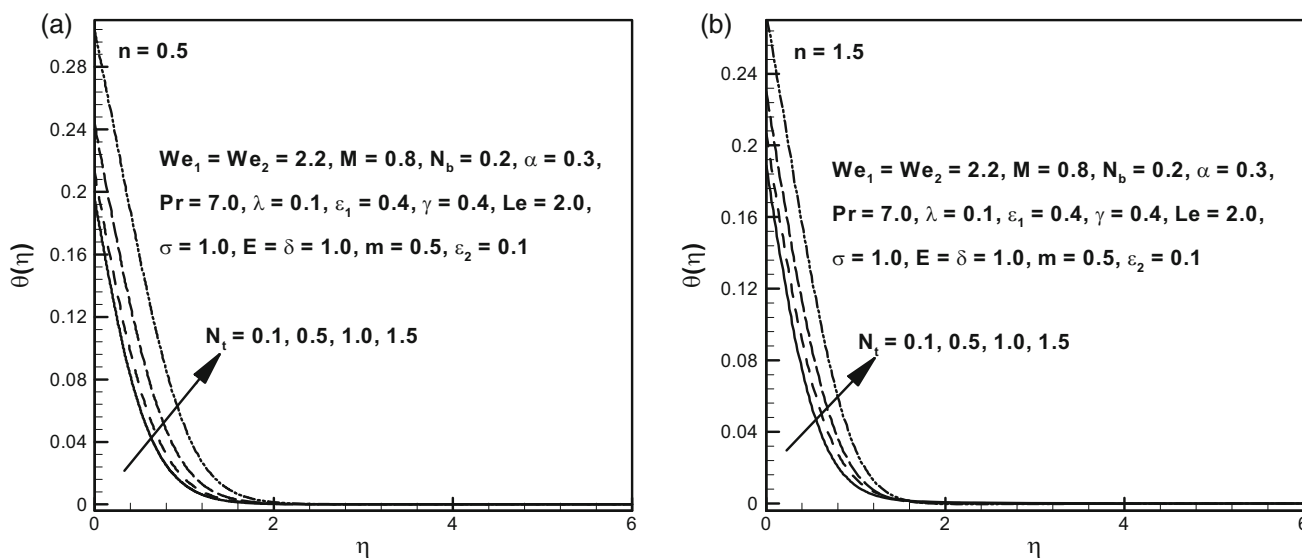


Figure 6. Illustration of $\theta(\eta)$ for various values of N_t for (a) shear-thinning and (b) shear-thickening liquids.

velocity of the cross fluid. Physically, as we increase M Lorentz’s force is enhanced, due to which the velocity of the cross fluid decreases.

5.2 Nanofluid temperature profiles

Figures 4–8 illustrate the aspects of various physical parameters on the temperature of the cross nanofluid for $n < 1$ and $n > 1$. Figures 4a and 4b represent the impacts of α on the temperature profile of the cross nanofluid. Through graphical data, the deteriorating behaviour of the cross fluid is detected while sketching the temperature profile. For constant values

of the involved physical parameters, a variation in the temperature of the cross nanofluid with variable conductivity ϵ_1 is presented in figures 5a and 5b. Graphical data show that the cross nanofluid temperature increases with increasing ϵ_1 . Figures 6a and 6b demonstrate the effects of N_t on the dimensionless temperature profile of the cross nanofluid. These figures show that the augmentation in N_t has the tendency to increase the temperature of the nanofluid. This mechanism of the cross nanofluid is physically practical because increasing the estimation of the N_t difference of the nanofluid temperature between the nanofluid at infinity and the heated fluid behind the sheet increases. The non-dimensional temperature of the

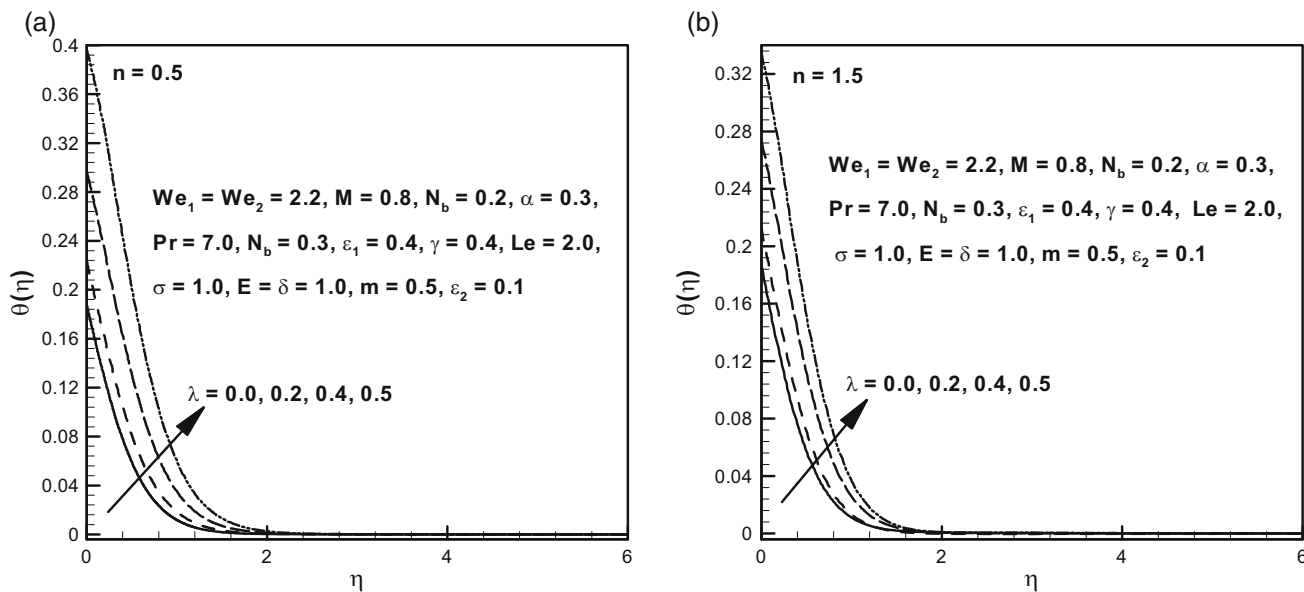


Figure 7. Illustration of $\theta(\eta)$ for various values of λ for (a) shear-thinning and (b) shear-thickening liquids.

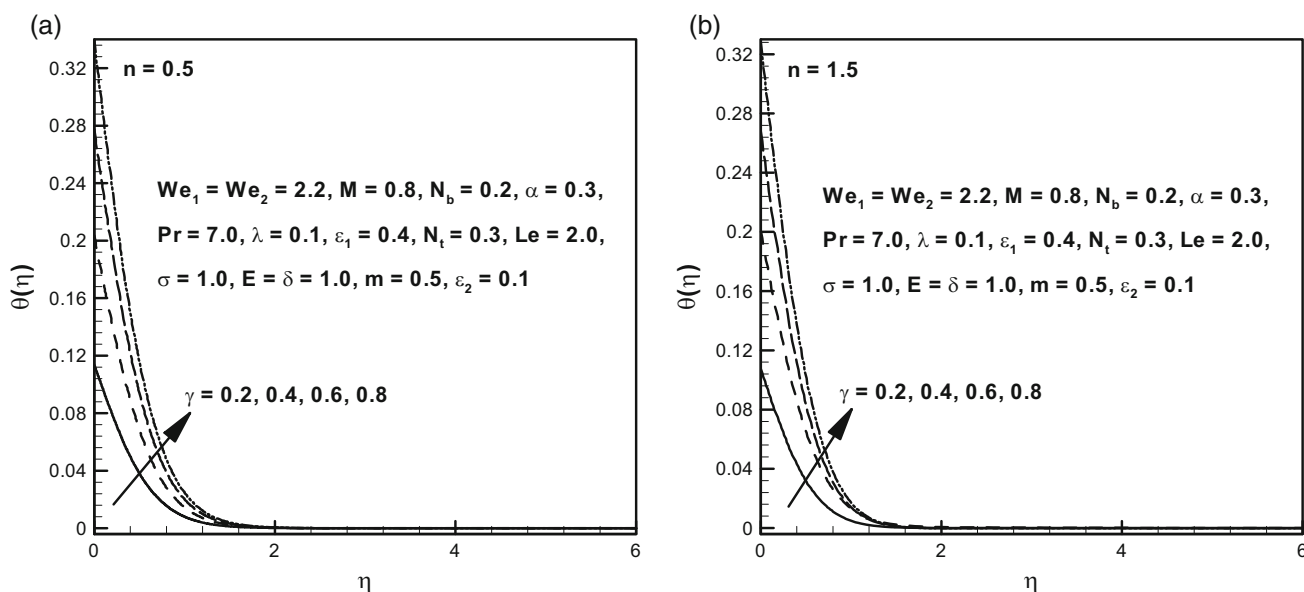


Figure 8. Illustration of $\theta(\eta)$ for various values of γ for (a) shear-thinning and (b) shear-thickening liquids.

cross nanofluid is sketched in figures 7a and 7b with the rising values of λ . As revealed from the graphical data, λ has a great impact on the temperature of the nanofluid, i.e. the temperature of the nanofluid is increased by an increase in λ . Figures 8a and 8b show the characteristics of γ on the temperature of the nanofluid. It is perceived from our graphical outcomes that for specific values of the involved physical parameter, a significant raise in temperature of the nanofluid is exhibited for augmented values of γ . The physical reason behind this trend of γ is that less resistance is faced by the thermal wall which

causes an enhancement in convective heat transfer to the fluid.

5.3 Nanofluid concentration profiles

Figures 9–13 demonstrate the impact of non-dimensional physical parameters on the concentration of the nanofluid. Characteristics of nanofluid concentration corresponding to activation energy E are shown in figures 9a and 9b. It is remarkable that an increment E has a tendency to increase the nanofluid concentration.

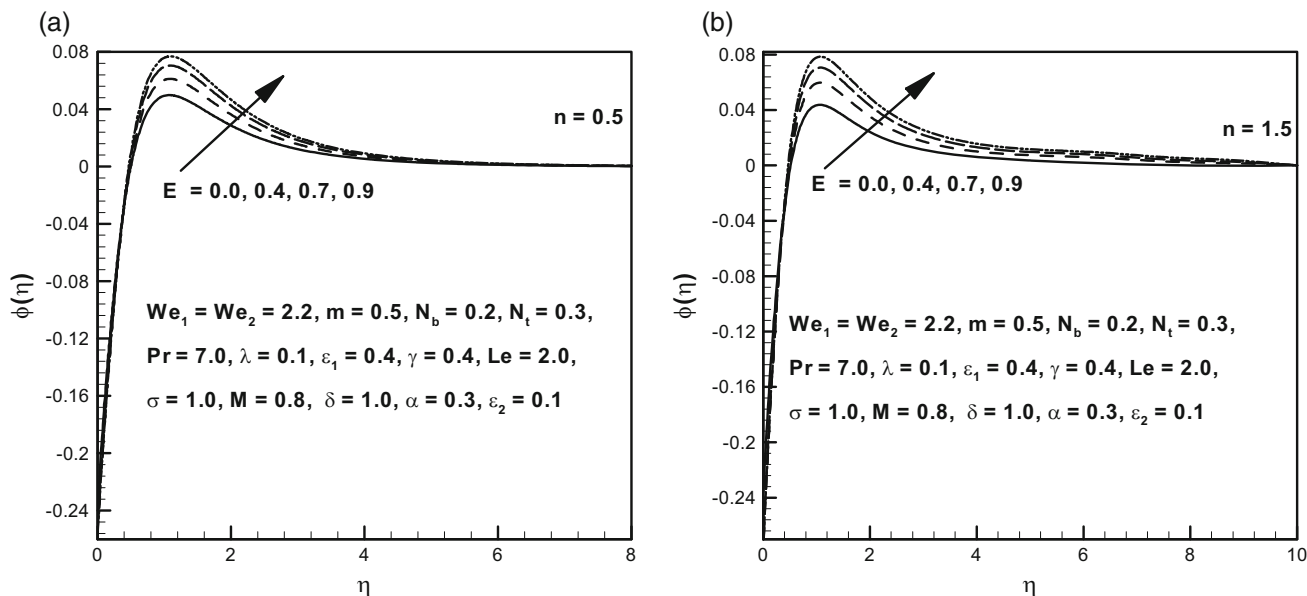


Figure 9. Illustration of $\phi(\eta)$ for various values of E for (a) shear-thinning and (b) shear-thickening liquids.

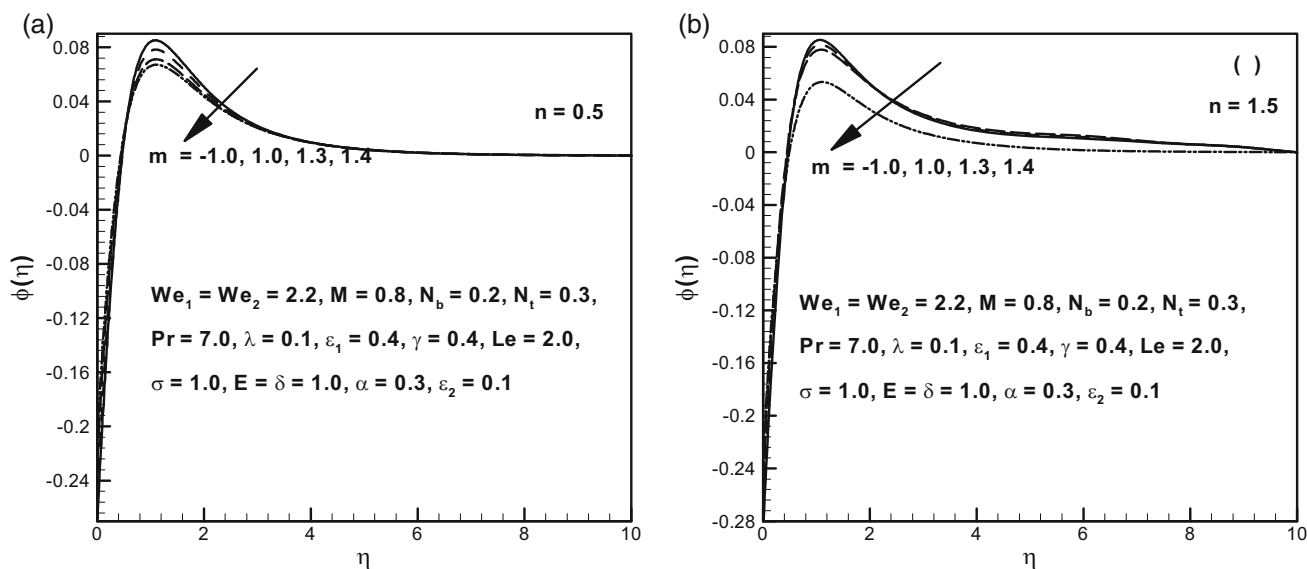


Figure 10. Illustration of $\phi(\eta)$ for various values of m for (a) shear-thinning and (b) shear-thickening liquids.

The variations in nanofluid concentration distribution are plotted in figures 10a and 10b for distinct values m . It is observed in these figures that an augmentation in m provides a deterioration in nanofluid concentration. Most significant features of figures 11a, 11b and 12a, 12b are to bring out aspects of N_b and N_t for the concentration of the nanofluid. We inferred that an increase in N_t increases the nanofluid concentration while a reverse trend is detected for N_b . Moreover, it is perceived that physically, an increase in the magnitude of N_b corresponds to the rise in the rate at which nanoparticles in the base liquid move in

random directions at different velocities. This movement of nanoparticles augments the transfer of heat, and therefore, declines the concentration profile. To investigate the aspects of ϵ_2 on the concentration profile, we have plotted figures 13a and 13b. These figures reveal that the concentration profile enhances as the value of ϵ_2 is increased.

5.4 Quantity of physical interest

Table 2 is presented to determine the achieved outcomes of the heat transport rate for the cross nanofluid. Table 2

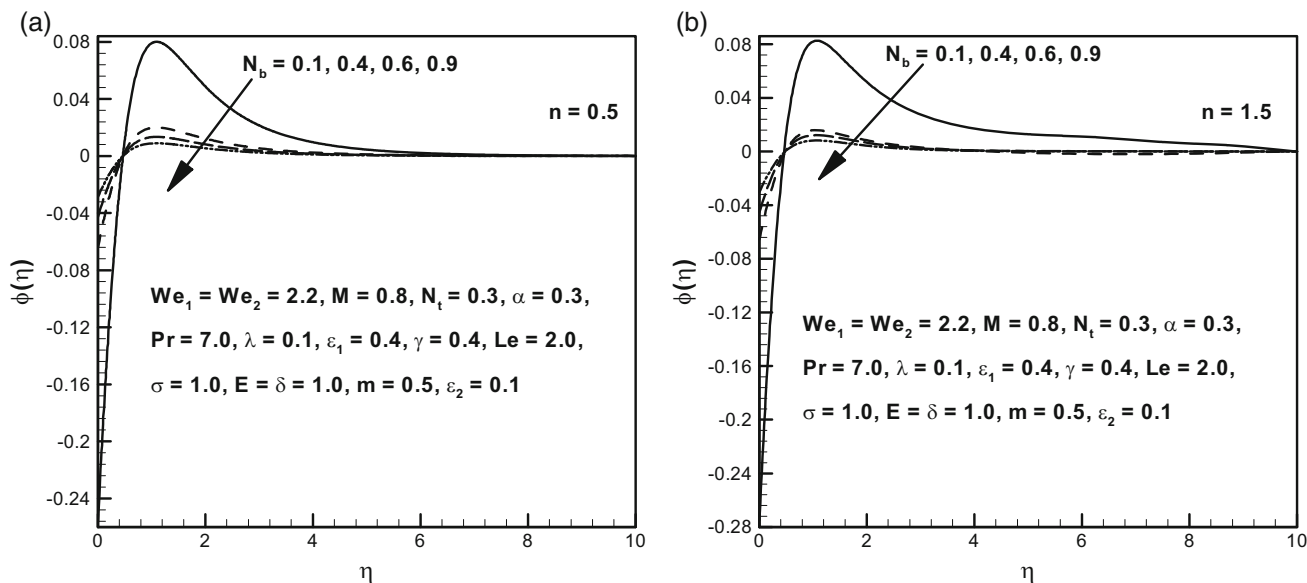


Figure 11. Illustration of $\varphi(\eta)$ for various values of N_b for (a) shear-thinning and (b) shear-thickening liquids.

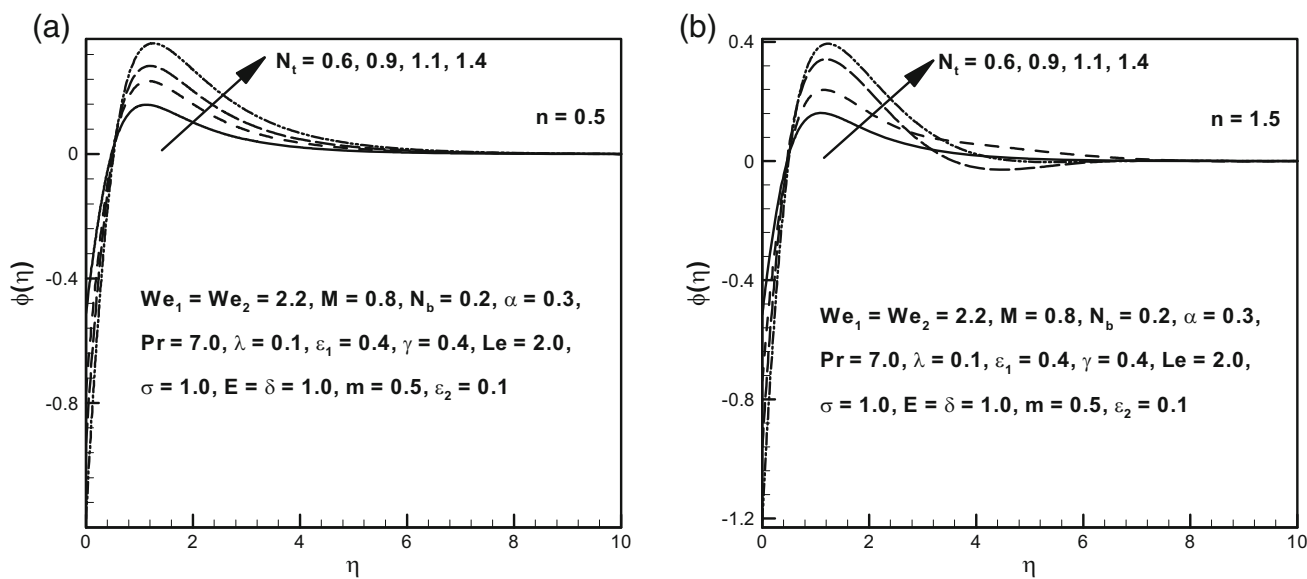


Figure 12. Illustration of $\varphi(\eta)$ for various values of N_t for (a) shear-thinning and (b) shear-thickening liquids.

reveals that the magnitude of the heat transport rate deteriorates for augmented values of δ , ϵ_1 , ϵ_2 , σ and N_t while it rises for Pr and E .

6. Main outcomes

A detailed characterisation of boundary layer flow, heat and mass transport of the cross nanofluid is studied here to elucidate the aspects of the chemical process. Moreover, variable diffusivity phenomenon is utilised to describe the mass transport mechanism. Numerical

computation is employed for the modelled equations. Outcomes of this work are presented in the form of graphical and tabular data. The findings can be summarised as follows:

- Temperature of the cross nanofluid is an increasing function of N_t .
- Higher estimation of λ provides larger temperature of the cross nanofluid.
- An increment in α demonstrates decays in $\theta(\eta)$.
- $\varphi(\eta)$ is increased with increasing values of M .

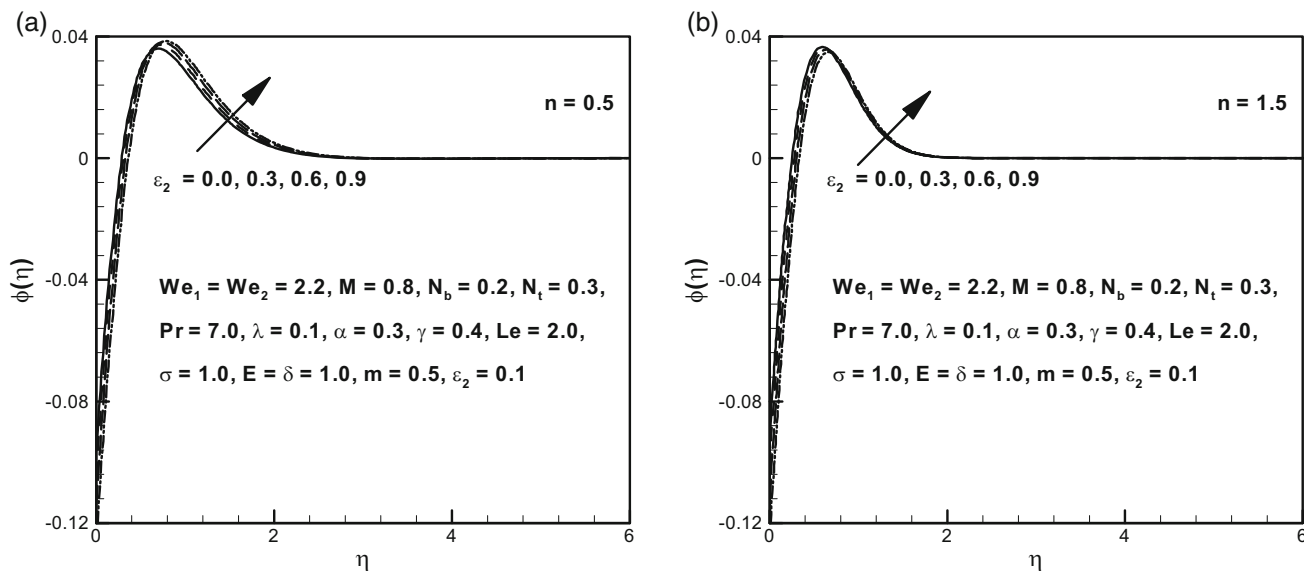


Figure 13. Illustration of $\varphi(\eta)$ for various values of ε_2 for (a) shear-thinning and (b) shear-thickening liquids.

Table 2. Numerical values of the rate of heat transport $(Re_x)^{-1/2}Nu_x$ for distinct values of escalating parameters when $M = 0.8$, $We_1 = We_2 = 2.2$, $Le = 2.0$, $N_b = 0.2$, $\alpha = 0.3$ and $\gamma = 0.5$.

Pr	E	δ	ε_1	ε_2	σ	N_t	$(Re_x)^{-1/2}Nu_x$
1.0	1.0	1.0	0.4	0.1	1.0	0.3	0.270327
1.2	–	–	–	–	–	–	0.280799
1.4	–	–	–	–	–	–	0.289058
1.6	1.1	–	–	–	–	–	0.294705
–	1.2	–	–	–	–	–	0.294715
–	1.4	–	–	–	–	–	0.294731
–	–	1.5	–	–	–	–	0.294678
–	–	2.0	–	–	–	–	0.294662
–	–	2.5	–	–	–	–	0.294648
–	–	–	0.5	–	–	–	0.294393
–	–	–	0.8	–	–	–	0.290153
–	–	–	1.0	–	–	–	0.287282
–	–	–	–	0.3	–	–	0.294648
–	–	–	–	0.6	–	–	0.294584
–	–	–	–	0.9	–	–	0.294528
–	–	–	–	–	1.2	–	0.294667
–	–	–	–	–	1.5	–	0.294626
–	–	–	–	–	1.8	–	0.294585
–	–	–	–	–	–	0.5	0.293404
–	–	–	–	–	–	0.7	0.292119
–	–	–	–	–	–	0.9	0.290737

- Concentration of the cross magnetonano fluid increases for increasing values of E .
- $\varphi(\eta)$ decays via m .
- Profiles of concentration decrease for escalating values of m and σ .

References

- [1] W A Khan, M Khan and R Malik, *PLoS ONE* **9**(8), e10510 (2014)
- [2] A K Gupta and S S Ray, *Powder Technol.* **279**, 282 (2015)
- [3] M Sheikholeslami and R Ellahi, *Int. J. Heat Mass Transf.* **89**, 799 (2015)
- [4] M Khan and W A Khan, *AIP Adv.* **5**, 107138 (2015)
- [5] N Sandeep, B R Kumar and M S J Kumar, *J. Mol. Liq.* **212**, 585 (2015)
- [6] M Khan and W A Khan, *AIP Adv.* **6**, 025211 (2016)
- [7] Rizwan ul Haq and Z H Khan, *J. Mol. Liq.* **221**, 298 (2016)
- [8] M Khan and W A Khan, *J. Braz. Soc. Mech. Sci. Eng.* **38**(8), 2359 (2016)
- [9] M Khan, W A Khan and A S Alshomrani, *Int. J. Heat Mass Transf.* **101**, 570 (2016)
- [10] S U Rahman, R Ellahi, S Nadeem and Q M Zaigham Zia, *J. Mol. Liq.* **218**, 484 (2016)
- [11] C S K Raju, N Sandeep and V Sugunamma, *J. Mol. Liq.* **222**, 1183 (2016)
- [12] N C Peddisetty, *Pramana – J. Phys.* **87**: 62 (2016)
- [13] T Hayat, M Waqas, S A Shehzad and A Alsaedi, *Pramana – J. Phys.* **86**, 3 (2016)
- [14] T Hayat, M Rashid, M Imtiaz and A Alsaedi, *Int. J. Heat Mass Transf.* **113**, 96 (2017)
- [15] M Khan, L Ahmad and W A Khan, *J. Braz. Soc. Mech. Sci. Eng.* **39**(11), 4475 (2017)
- [16] T Hayat, M Javed, M Imtiaz and A Alsaedi, *Eur. Phys. J. Plus* **132**, 132 (2017)
- [17] B J Gireesha, B Mahanthesh and K L Krupalakshmi, *Results Phys.* **7**, 4340 (2017)
- [18] M Khan, M Irfan and W A Khan, *Eur. Phys. J. Plus* **132**, 517 (2017)

- [19] N Sandeep, *Adv. Powder. Technol.* **28**, 865 (2017)
- [20] W A Khan, A S Alshomrani, A K Alzahrani, M Khan and M Irfan, *Pramana – J. Phys.* **91**: 63 (2018)
- [21] M Sheikholeslami, *J. Mol. Liq.* **266**, 495 (2018)
- [22] S Saha Ray and S Sahoo, *Comput. Math. Appl.* **75**(7), 2271 (2018)
- [23] A S Alshomrani, M Z Ullah and S S Capizzano, *Arab. J. Sci. Eng.* **44**, 579 (2018)
- [24] M Sheikholeslami, *J. Mol. Liq.* **263**, 472 (2018)
- [25] T Hayat, H Khalid, M Waqas and A Alsaedi, *Comput. Methods Appl. Mech. Eng.* **341**, 397 (2018)
- [26] A K Gupta and S Saha Ray, *Chaos Solitons Fractals* **116**, 376 (2018)
- [27] M Irfan, M Khan, W A Khan and M Ayaz, *Phys. Lett. A* **382**(30), 1992 (2018)
- [28] A K Gupta and S Saha Ray, *J. Comput. Nonlinear Dynam.* **12**(4), 041004 (2017)
- [29] S. Saha Ray and A K Gupta, *Appl. Math. Comput.* **266**, 135 (2015)
- [30] W A Khan, M Ali, F Sultan, M Shahzad, M Khan and M Irfan, *Pramana – J. Phys.* **92**, 21 (2019)
- [31] M Khan, M Irfan and W A Khan, *Pramana – J. Phys.* **92**, 17 (2019)
- [32] W A Khan, M Khan and A S Alshomrani, *J. Mol. Liq.* **223**, 1039 (2016)
- [33] W A Khan, A S Alshomrani and M Khan, *Results Phys.* **6**, 772 (2016)
- [34] M I Khan, M Waqas, T Hayat, M I Khan and A Alsaedi, *J. Mol. Liq.* **246**, 259 (2017)
- [35] M I Khan, M Waqas, T Hayat, M I Khan and A Alsaedi, *J. Braz. Soc. Mech. Sci. Eng.* **39**(11), 4571 (2017)
- [36] W A Khan, M Irfan, M Khan, A S Alshomrani, A K Alzahrani and M S Alghamdi, *J. Mol. Liq.* **234**, 201 (2017)
- [37] M Mustafa, J A Khan, T Hayat and A Alsaedi, *Int. J. Heat Mass Transf.* **108**, 1340 (2017)
- [38] W A Khan, M Ali, F Sultan, M Shahzad, M Khan and M Irfan, *Pramana – J. Phys.* **92**, 16 (2019)
- [39] P D Ariel, *Comput. Math. Comput.* **266**, 135 (2015)